Annals of Nuclear Energy 69 (2014) 57–61

Contents lists available at ScienceDirect

Annals of Nuclear Energy

journal homepage: www.elsevier.com/locate/anucene

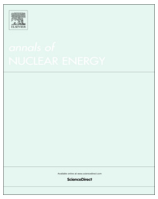

Technical note

n/γ Pulse shape discrimination comparison of EJ301 and EJ339A liquid scintillation detectors

Can Liao [*], Haori Yang

Department of Nuclear Engineering & Radiation Health Physics, Oregon State University, 3451 SW Jefferson Way, Corvallis, OR 97331, United States

ARTICLE INFO

Article history:
Received 21 January 2014
Accepted 30 January 2014
Available online 21 February 2014

Keywords:
Neutron detector
Liquid scintillation detector
Pulse shape discrimination

ABSTRACT

In this work, we evaluated the neutron-gamma discrimination capability of EJ301 and EJ339A liquid scintillation detectors via the pulse shape discrimination (PSD) method. Both simulation and experimental results are reported. The Geant4 simulation toolkit was used to model the scintillation process inside the scintillator, for neutron and gamma events, respectively. For the experiments, a high-speed digitizer was used to acquire data, which was then processed in MATLAB. This work compared the PSD performance of two liquid scintillation detectors and demonstrated the capability of Geant4 with regard to simulation of pulse shape.

1. Introduction

Liquid scintillation detectors are widely used in measurements of both neutrons and gamma rays because of their sensitivity to both radiations (Colonna et al., 1996; Tilquin et al., 1995; Wolski et al., 1995; Klein and Neumann, 2002). Therefore, their capability of pulse shape discrimination (PSD) is a crucial feature to distinguish between neutron and gamma events.

In most scintillators, the scintillation production shows a time response described by a superposition of several exponential decay components with different decay time constants instead of a simple exponential decay. This is described in the following equation:

$$f = Ae^{-t/\tau_f} + Be^{-t/\tau_s} \tag{1}$$

where f stands for the light yield, τ_f is the decay constant of fast component and τ_s is the decay constant of slow component.

According to the Birk's Law, the light yield per path length is not linear at high loss rates (heavy charged particles). The loss of linearity is due to the recombination and quenching effects between the excited molecules and the surrounding substrate. (Birks, 1964). However, quenching does not significantly affect the slow florescence component. This means that although heavy particle interaction gives rise to a relatively larger slow component than an electron interaction, the total number of photoelectrons are not necessarily larger for the particle (Söderström, 2009). Thus, the fraction of light that appears in the slow component is larger for heavier charged particles, which results in pulses produced by heavier charged particles, such as protons and alphas having larger tails than those caused by lighter particles, i.e., electrons. It serves as the basis of the PSD method aiming to distinguish pulses induced by different types of particles.

The PSD technique has been widely used for various applications over the past decade (Yamazaki et al., 2011; Ranucci et al., 1998). Recently, it has drawn great interest in the areas of nuclear nonproliferation and homeland security (Enqvist et al., 2008). Various techniques and algorithms to accurately distinguish between desired neutron signal and undesired gamma background have been developed and evaluated (Esmaeili-sani et al., 2012; Flaska and Pozzi, 2007). Currently, common PSD techniques used with the liquid scintillation detector utilize one of the following three analog algorithms (Ranucci, 1995):

(1) Rise-time inspection.
(2) The zero-crossing method.
(3) Charge comparison.

In this paper, we present a study on the PSD feature of two liquid scintillation detectors, EJ301 and EJ339A, using both Monte-Carlo simulations and experiments.

2. Geant4 simulation

2.1. Optical process simulation setup

The Geant4 toolkit package is a good tool to study the PSD performance of a detector (Agostinelli et al., 2003). In order to obtain the pulse shape information after interaction between

---

[*] Corresponding author. Tel.: +1 801 7396763.
E-mail address: liaoc@onid.orst.edu (C. Liao).

http://dx.doi.org/10.1016/j.anucene.2014.01.039
0306-4549/

Table 1
Major properties of EJ339A and EJ301.

Detector	EJ339A	EJ301
Light output	65%	78%
No. of blue photons per electron (MeV)	10,000	12,000
Decay, fast component (Time/ns)	3.7	3.2
Decay, slow component (Time/ns)	20	32.3
Density, g/cc (20 °C)	0.92	0.874
Scintillation liquid	Trimethylbenzene	Xylene
Birk's constant (mm/MeV)	0.102	0.143

the incident radiation and the scintillator, the optical scintillation process has to be integrated into the simulation. In Geant4, there is no smooth transition between optical photons and gamma particle classes. Thus, a separate physics process for optical photons has to be specified, which describes the scintillation process in the detector set-up. A separate class named G4OpticalPhoton was used to model the production and transport of optical photons.

In the DetectorConstruction class, scintillation features need to be defined according to the properties of the particular scintillation material, such as emission spectrum, light output, and number of photons generated per 1 MeV of electron energy deposition. These properties of EJ301 and EJ339A are respectively shown in Table 1 and Fig. 1 (EJ-339 data sheet; EJ-301 data sheet). Furthermore, since the simulation includes the scintillation process caused by heavily charged particles, the quenching effect is added according to Birk's Law. In Geant4, Birk's Law was implemented by adding G4EmSaturation into the PhysicsList class and setting Birk's constant in the DetectorConstruction class. EJ301 is identical to NE213, a xylene-based liquid scintillator manufactured by Nuclear Enterprises, Ltd., Winnepeg, Canada. The Birk's constant is reported by R. L. Craun and D. L. Smith (Craun and Smith, 1970). The Birk's constant of EJ339A is found in Back et al. (2008).

Moreover, as described in the introduction, the fraction of light that appears in the slow component differs for different particles and serve as the basis of PSD. Therefore, this feature has to be specified in the simulation. In Geant4, the method SetScintillationExcitationRatio can be called for each scintillation process to specify the relative strength of the fast component as a fraction of total scintillation yield. Before doing this, the value of variable scintillationByParticleType is set to be true so that the scintillation process can be defined for each particle type. The values of excitation ratios are estimated by Ranucci et al. (1998).

In order to obtain the pulse shape information through the simulation, the time response of the scintillation process is required. This is achieved by writing the time when each optical photon is collected by the cathode of a photomultiplier tube (set to be a sensitive detector in Geant4) to an output file. EventID and ParentID, which are built-in parameters available in the Geant4, are also recorded to distinguish the optical photons generated by different incident particles.

2.2. PSD algorithm

As mentioned in the introduction, the tails of the pulses for heavier particles are stronger than those for lighter particles. Since neutron scattering pulses are actually generated by recoil protons, they have larger tails than gamma pulses. Charge comparison is a used PSD algorithm. In this algorithm, each pulse is integrated via two separate routes. The first integration, A_1, called the total integral, is from the beginning to an optimized end point of the tail. The second integral, A_2, taken from a certain starting position on the tail after the pulse's maximum to the same end point as used for the total integral, is called the tail integral. The ratio of the rail integral to the total integral, R, is used to distinguish events resulting from different particles (Ranucci, 1995) (Fig. 2). In our work, we chose this charge comparison algorithm as the main algorithm to use when inspecting the PSD feature.

2.3. Pulse imitation and simulation results

In the simulation for each detector, a mono-energetic gamma ray beam with energy of 662 keV and a mono-energetic neutron beam with energy of 4 MeV are utilized. The time response of the scintillation light yield can be estimated by taking a histogram of the arrival times of optical photons that reached the cathode of the PMT. However this histogram is not a good representation of the real pulse shape since the effect of PMT is neglected. To imitate the real pulse shape, we convolve the time response of the scintillation light yield and the single-electron time response (Söderström et al., 2008). The single-electron response can be described mathematically as:

$$V = \frac{t}{\tau} e^{-\frac{t}{\tau}} \tag{2}$$

where τ is the rise time of the PMT (Choong, 2009). Fig. 3 illustrates the single-electron response of the two PMTs coupled on EJ339A and EJ301. The rise time of ETEL-9390 KB (EJ339A) is 13 ns, and the rise time of RCA-8575 (EJ301) is 2.1 ns, which are reported respectively in their datasheets.

After obtaining the pulse shape, the tail integral and total integral are then calculated as discussed in Section 2.2. For EJ339A, the tail integral starts 55 ns after the point whose amplitude is half of the maximum at the first edge, and the total integral is calculated from the beginning to 100 ns. For EJ301, the tail integral starts 15 ns after the point whose amplitude is half of the maximum at the first edge, and the total integral is calculated in the same way. Different starting point are used for EJ301 and EJ339A because the pulse width are different due to different PMTs and different decay constants. The tail-to-total ratio are then calculated. The tail integral versus total integral plots of EJ339A and EJ301 pulses are shown in Fig. 4. Additionally, distributions of the tail-to-total ratio are produced for the two detectors (see Fig. 5). As shown in the results, obvious separation between neutron pulses and gammas pulses can be observed in both figures as expected. Thus, simulation results indicate good PSD capability of both

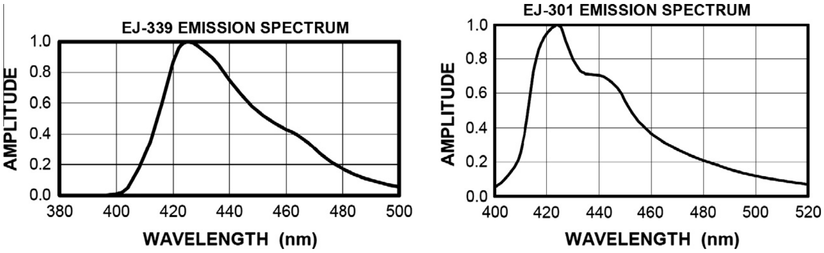

Fig. 1. EJ-339A and EJ-301 emission spectrums.